Hydration and OH^-/Br^- Conduction Properties of Fluorene-Thiophene-Based Anion Exchange Thin Films Tethered with Different Cations

Fangfang Wang [†], *Shusaku Nagano* [‡], *Mitsuo Hara* [§], *Yuki Nagao* [†]*

[†]School of Materials Science, Japan Advanced Institute of Science and Technology, 1-1 Asahidai, Nomi, Ishikawa 923-1292, Japan

[‡]College of Science, Rikkyo University, Tokyo 171-8501, Japan

[§]Department of Molecular & Macromolecular Chemistry, Nagoya University, Nagoya 464-8603, Japan

*Email: ynagao@jaist.ac.jp, Phone: +81(Japan)-761-51-1541

KEYWORDS: Fuel cells, temperature dependence of OH^- conductivity, thin film, water uptake, cation

ABSTRACT

After trimethylammonium (TMA) and N-methylpiperidinium (Pip) functionalized fluorene-thiophene-based anion conductive polymers were synthesized for this work, the effect of cationic groups on hydration and conduction properties of OH^-/Br^- form fluorene-thiophene-based thin films were investigated. Fluorene-thiophene-based thin film carrying TMA showed superior OH^- conductivity to that functionalized with Pip, above 10^{-2} S cm^{-1} at 25 °C under 95% relative humidity (RH), because it had higher ion exchange capacity (IEC), lower hydrophobicity, and smaller size of TMA. In situ temperature dependence OH^- conductivity measurement process for the thin film form was established under different temperatures and 90% RH. The activation energies (E_a) of OH^- conduction for thin films carrying TMA and Pip are 33.2 kJ mol^{-1} and 35.7 kJ mol^{-1}. The E_a of OH^- conduction was independent of the cation. This is the first systematic study of hydration and OH^- conduction properties of anion exchange thin films.

1. INTRODUCTION

Fossil fuels are still the primary energy sources supporting modern society, but finding alternative energy sources is urgent because of fuel depletion and environmental pollution. Fuel cell technology provides a clean, highly efficient, and flexible alternative energy-generating system.[1] Research efforts in fuel cells, particularly anion exchange membrane fuel cells (AEMFCs) have increased considerably because of the potential of AEMFCs to use non-noble metal catalysts and provide higher oxygen reduction reaction (ORR) kinetics under alkaline conditions.[2]

Anion exchange thin film is a crucial component for AEMFCs. Anion exchange thin films serve as binders and ion conduction channels in a triple-phase interface, which is related to the electrochemical performance of AEMFCs. Understanding the properties of anion exchange thin films is crucially important for AEMFCs development. Nevertheless, the investigation of water uptake and conductivity of OH^- form anion exchange thin films remains challenging because the whole process from film preparation to measurement should be performed in a CO_2-free atmosphere. The available literature has mainly addressed the hydration and ion conduction of anion exchange thin films in halide or HCO_3^- forms.[3–6] Quaternized comb-shaped poly(p-phenylene oxide) (QA-PPO) thin films in Br^- form with different side chain lengths exhibit similar hydration number (λ) above 80% relative humidity (RH).[4] Shrivastava and co-authors demonstrated that higher Br^- and HCO_3^- conductivities than F^- conductivity were observed at λ of approximately 1.2–2 in commercial Fumasep Fumion FAA3 thin films.[3] Luo and co-authors investigated the hydration and morphology of anion exchange thin films with different backbones, side chains, and counter-anions. The findings shed light on the effects of backbone, side chain, and anion/cation types on the hydration and morphology of anion exchange thin films.[5] The properties

of OH^- form anion exchange thin films are largely unknown. Our earlier work found that the 273 nm-thick poly[(9,9-bis(6′-(N,N,N-trimethylammonium)-hexyl)-9*H*-fluorene)-alt-(1,4-benzene)] (PFB^+) film showed superior OH^- conductivity value (5.3×10^{-2} S cm^{-1} at 25 °C under 95% RH) compared to Br^- conductivity.[7] Nevertheless, some challenges remain for the systematic study of OH^- conduction and hydration of anion exchange thin films, especially the temperature dependent OH^- conductivity of anion exchange thin films. To overcome this obstacle, new anion conductive polymers were synthesized and investigated as thin film form. Furthermore, in situ temperature dependence of OH^- conductivity measurement process was developed to obtain the activation energy of OH^- conduction in thin films in this work.

The design of anion conductive polymer is based on the choice of backbone and cationic group. The cationic group is attached to the backbone or the side chain extending from the backbone.[8–16] The ideal anion conductive polymer should possess high OH^- conductivity, good mechanical and high stability properties even under high pH conditions. Fluorene-thiophene-based conjugated polymers have good film-forming properties and high chemical stability. Fluorene-based anion conductive polymers have been studied widely.[17–21] Therefore, the fluorene-thiophene-based copolymer was designed as the backbone for this work. The cationic group attached to the alkyl side chain can increase the conductivity and alkaline stability of anion conductive polymers markedly.[22,23] The ion conduction and hydration properties of anion conductive polymers are influenced by interaction between the counterion and cation.[3,24,25] Effects of the cationic group on the hydration and anion conduction properties of anion exchange thin film remain unclear. Trimethylammonium (TMA) and sterically hindered N-methylpiperidinium (Pip) are commonly used cationic groups because of their high OH^- conductivity, lower cost, and easier functionalization.[26] Therefore, fluorene-thiophene-based copolymer functionalized with TMA and

Pip via alkyl side chains were designed for this work. The chemical structures of poly[(9,9-bis(6′-(N,N,N-trimethylammonium)hexyl)fluorene)-alt-(3,3′-dihexyl-2,2′-bithiophene)] (PFT6-TMA) and poly[(9,9-bis(6′-(N-methylpiperidinium)hexyl)fluorene)-alt-(3,3′-dihexyl-2,2′-bithiophene)] (PFT6-Pip) are shown in Figure 1.

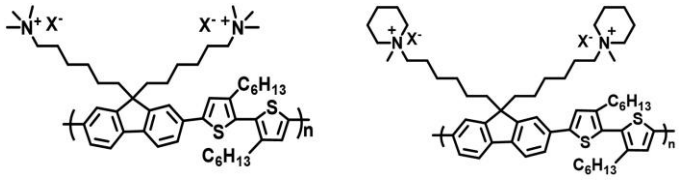

Figure 1. Chemical structures of PFT6-TMA and PFT6-Pip (X=OH and Br).

The objective of this work is to assess the hydration properties, anion conductive properties, and morphology of prepared fluorene-thiophene-based anion exchange thin films with different cationic groups and counter-anions, especially the properties of OH^- form thin films. The hydration and anion conductive properties of anion exchange thin films were investigated using in situ quartz crystal microbalance (QCM), in situ Fourier transform infrared spectroscopy (FTIR), and in situ impedance spectroscopy measurements taken under different RH. To analyze the morphology of anion exchange thin films, RH-controlled grazing-incidence small-angle X-ray scattering (GI-SAXS) was used. The TMA functionalized fluorene-thiophene-based anion exchange thin film exhibited high OH^- conductivity. Water uptake results reveal that counter-anion hydration is the dominant factor for the water uptake of fluorene-thiophene-based anion exchange thin film rather than cations. The relation between anion conductivity and water uptake of fluorene-thiophene-based anion exchange thin films suggests that OH^- conduction is strongly dependent on the number of water molecules. In both Br^- and OH^- forms, PFT6-TMA and PFT6-Pip thin films exhibited similar anion conduction activation energies.

2. EXPERIMENTAL SECTION

2.1 Materials

2,7-Dibromofluorene, 1,6-dibromohexane, tetrabutylammonium bromide (TBAB), bis(pinacolato)diboron, [1,1-bis(diphenylphosphino)ferrocene] dichloro palladium (II) ($PdCl_2$) (dppf), 5, 5'-dibromo-3, 3'-dihexyl-2, 2'-bithiophene, and tetrakis(triphenylphosphine) palladium (0) (Pd (PPh_3)$_4$) were purchased from Tokyo Chemical Industry Co., Ltd., Japan. Sodium hydroxide, dichloromethane, sodium chloride, sodium bicarbonate, 2-propanol, magnesium sulfate anhydrous, dioxane, hexane, methanol, chloroform, tetrahydrofuran (THF), toluene, potassium carbonate, 30% trimethylamine solution, N-methylpiperidine, and diethyl ether were used as received from Fujifilm Wako Pure Chemical Corp., Japan.

2.2 Synthesis Process

The synthetic routes of monomer and polymers are shown in Scheme S1 and Scheme 1. 2,7-dibromo-9,9-bis(6′-bromohexyl) fluorene and 2,7-bis(4,4,5,5-tetramethyl-1,3,2-dioxaborolan-2-yl)-9,9-bis(6′-bromohexyl)fluorene were synthesized according to the literature.[27] Detailed synthesis and characterization information is shown in Supporting Information (Figure S1).

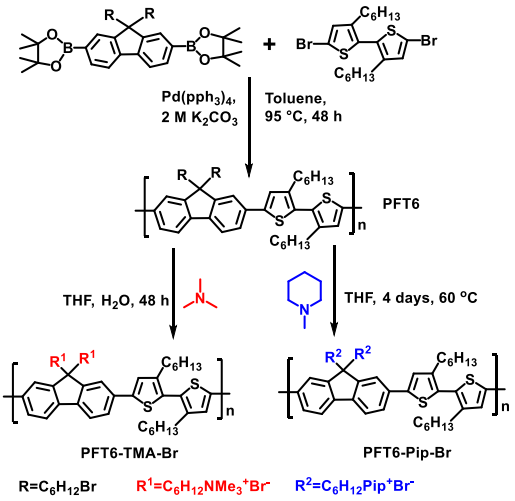

Scheme 1. Synthesis route of PFT6-TMA-Br and PFT6-Pip-Br.

Poly[(9,9-bis(6′-(N,N,N-trimethylammonium)hexyl)fluorene)-alt-(3,3′-dihexyl-2,2′-bithiophene)] bromide (PFT6-TMA-Br)

200 mg of poly[(9,9-bis(6′-bromohexyl)fluorene)-alt-(3,3′-dihexyl-2,2′-bithiophene)] (PFT6) was dissolved in 2 mL of THF. Then 1 mL of 30% trimethylamine solution was added to the mixture. After the precipitate appeared, 2 mL of DI water was added to the reaction mixture. The reaction was conducted at room temperature for 48 h. After removal of solvents, the concentrate was dissolved in methanol and precipitated in diethyl ether. After drying under reduced pressure, PFT6-TMA-Br was obtained. (Yield: 200 mg, 88%)

Poly[(9,9-bis(6′-(N-methylpiperidinium)hexyl)fluorene)-alt-(3,3′-dihexyl-2,2′-bithiophene)] bromide (PFT6-Pip-Br)

200 mg of PFT6 was dissolved in 5 mL of THF. 8 mL of N-methylpiperidine was added to the solution. The mixture was stirred at 60 °C for 4 days under the protection of Ar. Afterward, the solvent was evaporated. The concentrate was dissolved in methanol and was precipitated in diethyl ether. The product was dried under vacuum overnight to obtain PFT6-Pip-Br. (Yield: 197 mg, 80%)

2.3 Characterization

Detailed experiment-related information about nuclear magnetic resonance (^{1}H NMR), gel permeation chromatography (GPC), attenuated total reflection FTIR (ATR-FTIR) spectroscopy, thermogravimetric analyzer (TGA), ion exchange capacity (IEC), scanning Electron Microscope and Energy Dispersive X-ray Spectroscopy (SEM-EDX), and p-Polarized multiple angle incidence resolution spectrometry (pMAIRS) is presented in Supporting Information.

2.4 Ion Exchange Process

PFT6-TMA-Br (or PFT6-Pip-Br) was immersed in degassed, and argon saturated 1 M NaOH solution at room temperature for 48 h. Within 48 h, the NaOH solution was changed three times. Subsequently, PFT6-TMA and PFT6-Pip (in OH^- form) were washed by degassed ultra-pure water until the pH was neutral. The whole process of OH^- form PFT6-TMA and PFT6-Pip was conducted under the Ar/N_2 atmosphere. PFT6-TMA-Br (or PFT6-Pip-Br) was immersed in 1 M $NaHCO_3$ solution at room temperature for 48 h. Within 48 h, the $NaHCO_3$ solution was changed three times. Subsequently, PFT6-TMA and PFT6-Pip (in HCO_3^- form) were washed by ultra-pure water until the pH was neutral. The OH^- and HCO_3^- forms of PFT6-TMA and PFT6-Pip-based anion conductive polymers were designated as PFT6-TMA-OH, PFT6-TMA-HCO_3, PFT6-Pip-OH, and PFT6-Pip-HCO_3.

2.5 Thin Film Preparation

To obtain solution, PFT6-TMA and PFT6-Pip in different anion forms were dissolved in methanol. Si, Au-coated QCM substrates (Seiko EG&G Co., Ltd.), and SiO_2 substrates were used to prepare thin films for this study by spin-coating (ACT-200; Active Co. Ltd.). The substrates were cleaned with 2-propanol before spin-coating. The surface hydrophilicity was obtained using the vacuum plasma system (Cute-MP; Femto Science). Thin film thickness was analyzed using a white-light interferometric microscope (BW-S506; Nikon Corp.). The preparation and all sample transfers of OH^- form thin films were conducted under a N_2 atmosphere. The thin films for water uptake measurement, conductivity measurement, and in situ FTIR measurements were approximately 480 nm thick. Thin films were 505 nm thick for GI-SAXS measurements.

2.6 Water Uptake Measurements

Water uptake of PFT6-TMA-Br, PFT6-TMA-OH, PFT6-Pip-Br, and PFT6-Pip-OH thin films was measured using an in situ quartz crystal microbalance (QCM) system under 25 °C and various

RH conditions. Au-coated QCM substrates were connected to an oscillation circuit with a frequency counter (53131-A; Agilent Technologies Inc.). A home-made chamber with a high-resolution RH sensor was used to hold the QCM substrates. A dry N_2 and humidity controller (BEL Flow; MicrotracBEL Corp.) were used to produce the various RH conditions. After setting the RH value, the RH inside the home-made chamber increased steadily by controlling the N_2 and water vapor through humidity controller. Once reaching the desired RH, the thin films were kept in this RH condition for enough time to reach equilibrium for water adsorption. Besides, the frequency was recorded when the monitored frequency value was stable within 10 minutes, and this stable frequency was used to calculate the water uptake of thin film to make sure the hydrated water of the thin film has been reached the equilibrium under fixed RH. The water uptake of thin films during humidification and dehumidification process was measured from 0% to 95% RH, and then back to 0% RH. Frequencies of substrates before and after film coating were recorded under dry conditions. Dry film mass is obtainable using the following Sauerbrey equation.

$$\Delta m = \frac{S\times\sqrt{\rho\mu}}{2\times F^2}\times(-\Delta F) \qquad (1)$$

Therein, S represents the electrode surface area. Also, ρ stands for quartz density, μ denotes the quartz shear modulus, and F expresses the fundamental frequency of the QCM substrate. Water uptake (WU) was calculated using the following equation.

$$WU = \frac{m}{m_0} - 1 \qquad (2)$$

In that equation, m stands for the mass of the film under each humidity, m_0 represents the mass of film at the dry condition.

$$\lambda = (\frac{m}{m_0} - 1)\times\frac{EW}{M_{H_2O}} \qquad (3)$$

In equation (3), M_{H_2O} is the molecular weight of water molecules, and EW is equivalent weight of PFT6-TMA and PFT6-Pip.

2.7 Hydration properties of thin films

Hydration properties of the prepared anion exchange thin films were obtained from in situ FTIR measurements taken under various RH conditions**.** Si wafer (E&M Corp) with thin film was placed in a home-made chamber. Transmission IR spectra were taken using an FTIR spectrometer (Nicolet 6700; Thermo Fisher Scientific Inc.). A precise dew point generator (me-40DP-2PW; Micro Equipment Inc.) was used to generate various RH. Smoothing processing was applied to improve visibility. Origin software (2020b) was used to deconvolute the -O-H stretching vibration band of water.

2.8 Morphology of thin films

The morphology of PFT6-TMA-Br and PFT6-Pip-Br thin films was obtained by RH-controlled GI-SAXS conducted on an X-ray diffractometer (FR-E; Rigaku Corp.) with an R-AXIS IV two-dimensional detector. A humidity-controlled cell with Lumirror® windows on the goniometer and vertical stage (ATS-C316-EM/ALV-3005–HM; Chuo Precision Industrial Co. Ltd.) was used to hold thin films. The wavelength of X-ray source radiated by Cu Kα was 0.1542 nm, with beam size of approximately 300 μm × 300 μm. Nitrogen gas and water vapor were used to obtain 0% RH and 95% RH. The incident angle of the X-ray beam was adjusted to 0.20°–0.22° for measurements. The camera length was set to 300 mm.

2.9 Anion conductivity measurements

The anion conductivity of PFT6-TMA-Br, PFT6-TMA-OH, PFT-TMA-HCO_3, PFT6-Pip-Br, PFT6-Pip-OH, and PFT6-Pip-HCO_3 thin films was measured by impedance spectroscopy using a

frequency response analyzer (SI1260; Solartron Analytical) equipped with a high-frequency dielectric interface (SI1296; Solartron Analytical). For Br^- and HCO_3^- conductivity measurements of PFT6-TMA and PFT6-Pip thin films, various RH and temperature conditions were controlled by humidity-temperature chamber (SH-222; Espec Corp.). For OH^- conductivity measurement of PFT6-TMA and PFT6-Pip thin films, thin film electrodes were placed in a sealed box with a high-resolution RH sensor. The temperature was controlled by humidity-temperature chamber (SH-222; Espec Corp.). A precise dew point generator (me-40DP-2PW; Micro Equipment Inc.) was used for humidity controlling and nitrogen protection. Anion conductivity (σ) was calculated as shown below.

$$\sigma = \frac{d}{Rlt} \qquad (4)$$

In that equation, *d* denotes the distance between the Au electrodes; *R* represents the resistance value from impedance. Also, *l* and *t* respectively stand for the length of the contact electrodes and film thickness.

The temperature-dependent anion conductivity of PFT6-TMA and PFT6-Pip thin films were measured from 20 °C to 50 °C under fixed RH=90%. The estimated activation energy of anion conduction was estimated according to the Arrhenius equation.

$$\sigma T = \sigma_0 exp\left(\frac{-E_a}{RT}\right) \qquad (5)$$

In that equation, *R* denotes the gas constant, *T* represents the temperature, and σ_0 is a pre-exponential factor.

3. RESULTS AND DISCUSSION

3.1 Characterization of Polymers

PFT6 was synthesized via the Pd $(PPh_3)_4$-catalyzed Suzuki coupling reaction. Figure S2 depicts the ^1H NMR spectrum of PFT6. The peaks around 7.40–7.80 ppm are assigned to the aromatic protons of fluorene ring. Thiophene ring protons were observed at 7.24 ppm. The signals around 0.40–3.40 ppm correspond to the protons of alkyl side chains. The weight average molecular weight (M_W) and PDI of PFT6 is 22 kg mol^{-1} and 2.1. The calculated number of repeat unit is around 26. PFT6-TMA-Br was synthesized by quaternization of precursor polymer with TMA; PFT6-Pip-Br was obtained after the quaternization of precursor polymer with Pip. The chemical structures of PFT6-TMA-Br and PFT6-Pip-Br were confirmed from ^1H NMR spectra. Figure S3 shows the ^1H NMR spectra of PFT6-TMA-Br and PFT6-Pip-Br. Compared with the ^1H NMR spectrum of PFT6, the new signal appeared around 3.00 ppm in PFT6-TMA-Br, corresponding to the methyl proton of TMA, indicating the introduction of TMA (Figure S3a). New proton signals from methyl groups of N-methylpiperidinium in PFT6-Pip-Br appeared around the position of 2.90 ppm, confirming the successful quaternization reaction (Figure S3b). Ion exchange capacity (IEC) values of PFT6-TMA-OH and PFT6-Pip-OH obtained from ^1H NMR by the ratio of aromatic protons and $-CH_3$ of cations were, respectively, 2.34 and 2.11 meq g^{-1}. IEC values of PFT6-TMA-OH and PFT6-Pip-OH obtained from the back-titration method were, respectively, 2.27 and 2.01 meq g^{-1}. The back-titrated IEC is consistent with the IEC value obtained from the ^1H NMR.

The ATR-FTIR spectra of the PFT6-TMA-Br and PFT6-Pip-Br are portrayed in Figure S4. The bands at 2854 and 2927 cm^{-1} in the spectra are associated with symmetric and asymmetric vibrations of methylene ($-CH_2$). The band at 1463 cm^{-1} is assigned to the stretching vibration of the aromatic ring. The –C–H stretching vibration of methyl groups appeared at 3016 cm^{-1}. Furthermore, the strong and broadband at around 3400 cm^{-1} appeared in PFT6-TMA-Br and PFT6-Pip-Br, which was attributed to the stretching vibration of –O–H of water. The high hydrophilicity

of PFT6-TMA-Br and PFT6-Pip-Br also indicates that the quaternization reactions were performed successfully. Thermogravimetric analyzer was used to illustrate the thermal stability of PFT6-TMA-Br and PFT6-Pip-Br. As shown in Figure S5, three stages of weight loss were found. The first stage, below 100 °C, was associated with the evaporation of absorbed water. The second weight-loss stage, between 200–300 °C, was attributable to degradation of the quaternary ammonium group. The third weight-loss stage at 400 °C might be ascribed to degradation of the polymer backbone. Thermal analysis results imply that the thermal decomposition temperature of PFT6-TMA-Br and PFT6-Pip-Br was higher than the common operation temperature of AEMFCs.

3.2 Water Uptake

The water uptake of anion exchange thin films provides insights into the relations between hydration conditions and ion transport properties. RH-controlled in situ QCM was used to investigate the water uptake of anion exchange thin films. Figure 2a shows the mass-based water uptake. As shown in Figure 2a, the water uptake of PFT6-TMA-OH thin film is slightly higher than that of PFT6-Pip-OH thin film due to the high IEC of PFT6-TMA-OH thin film. However, the OH^- conductivity is less relevant with the polymer mass. To understand the relationship between OH^- conduction and hydration properties of anion conductive polymers, another commonly used parameter λ was used to quantify water adsorption in the thin film. λ represents the number of water molecules per functional group. Figure 2b presents water uptake (λ) of PFT6-TMA and PFT6-Pip thin films under various RH at 25 °C. The water uptake increased gradually with increasing RH, irrespective of the counter-anions and cations. For both PFT6-TMA and PFT6-Pip thin films, the OH^- form exhibited a much higher water uptake than the Br^- form. Results suggest that the counter-anion strongly influences the water uptake of anion exchange thin films. The water uptake of ion conductive polymer is governed by complex interactions between water,

the hydrophilic cationic group, and the hydrophobic polymer matrix.[28] The higher water uptake of anion exchange thin film in OH^- form than in Br^- form at low hydration is attributed to the higher hydration energy and higher hydration number of OH^-.[29,30] The respective hydration energies of Br^- and OH^- are -335 and -520 kJ mol^{-1}.[29] At low hydration conditions, the water molecules were adsorbed onto cation–anion pairs because of a strong anion–cation interaction. Under the high RH region, the dissociation of cation-anion pair was enhanced as discussed for RH-controlled in situ FTIR results. According to Pearson's hard and soft acid–base (HSAB) theory, a large (soft) cation will bind strongly to large (soft) Br^- anion.[31] Under high water content, therefore, the OH^- dissociate from the cation more easily than Br^- ions, resulting in higher osmotic pressure and a correspondingly higher water uptake.[24,25,32] Both PFT6-TMA and PFT6-Pip thin films displayed similar water uptake (λ) in high hydration conditions in both Br^- and OH^- forms. In a high RH range, the water uptake (λ) was less affected by the cationic group. In case having the same anion form, similar osmotic pressure was obtained, corresponding to a similar water uptake (λ) result because the backbone of PFT6-TMA and PFT6-Pip is the same, except for the cationic group. Results suggest that the water uptake of the anion exchange thin films with the same polymer backbone is governed by the hydration properties of anion.

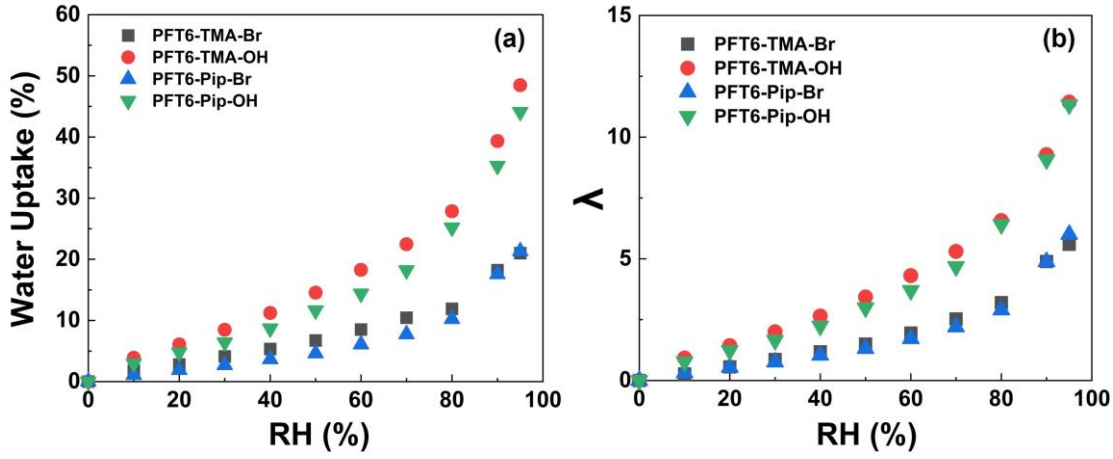

Figure 2. (a) Water uptake and (b) number of water molecules of PFT6-TMA and PFT6-Pip thin films as a function of RH at 25 °C.

Water adsorption hysteresis was observed in some anion exchange membranes.[24] The water uptake of PFT6-TMA-OH and PFT6-Pip-OH thin films during humidification and dehumidification process was measured. Figure S6 shows the number of water molecules of PFT6-TMA-OH and PFT6-Pip-OH thin films as a function of RH during humidification and dehumidification process. As shown in Figure S6, a small water adsorption hysteresis was found in PFT6-TMA-OH and PFT6-Pip-OH thin films in the whole RH range. The highest λ difference is 1.7 in PFT6-TMA-OH thin film between humidification and dehumidification at 90% RH.

3.3 Hydration Properties of Thin Films

Infrared spectroscopy can provide useful information about the hydration properties of ion conductive polymers.[33,34] Therefore, we performed RH-controlled in situ FTIR with a transparent mode to investigate interactions between polymer and H_2O in the PFT6-TMA-Br and PFT6-Pip-Br thin films. Figure 3 and Figure S7 depict the in situ FTIR spectra of PFT6-TMA-Br and PFT6-Pip-Br thin films as a function of RH. The bands were observed at 3415 and 1648 cm^{-1} corresponding to –O–H stretching vibration and H_2O bending vibration. As presented in Figure. 3a, 3b, and S7, the band intensity of –O–H stretching vibration and H_2O bending vibration increased concomitantly with increasing RH, suggesting the increased water adsorption of anion exchange thin films. The adsorbed water in the thin films can be mainly classified into bond water and bulk water. The –O–H stretching vibration band of bound water and bulk water can be observed around 3450 and 3250 cm^{-1}, respectively.[35,36] The abundance and relative abundance of bulk water and bound water in PFT6-TMA-Br thin film as a function of RH are shown in Figure S8. As shown in Figure S8a, both bond water and bulk water increased along RH. As shown in

Figure S8b, the fraction of bulk water increased, while the fraction of bound water decreased suggesting the enhanced bulk water under high RH range.

Based on earlier reports of the literature, interactions between cation, counter-anion, and water can be analyzed from the evolution of –C–H stretching vibration band in [–$N(CH_3)_3^+$].[34,37,38] Vico and co-authors investigated the ATR-FTIR spectra of polysulfone-based anion conductive polymer in the membrane form under various water contents. Decreased absorbance of the –C–H stretching vibration band in [–$N(CH_3)_3^+$] was observed with the increasing water content, which resulted from the weak interaction between the cation and counter-anion.[34] Vandiver and co-authors studied the ATR-FTIR spectra of polyethylene-b-poly(vinylbenzyl trimethylammonium) membrane as a function of RH. The position of the –C–H stretching vibration band in [–$N(CH_3)_3^+$] shifted to a high wavenumber, suggesting the increased amount of free water inside the membrane.[37] The –C–H stretching region of PFT6-TMA-Br and PFT6-Pip-Br thin films under various RH are presented in Figure 3c and 3d. The –C–H stretching vibration band is visible at 3006 cm^{-1} under 0% RH. The higher frequency shift and absorbance decrease for –C–H stretching vibration band in [-$N(CH_3)_3^+$] were observed with the increase of RH. This change indicates the enhanced force constant of –C–H bond in [–$N(CH_3)_3^+$]. Under dry conditions, cation–anion pairs were formed by strong interaction between [-$N(CH_3)_3^+$] and Br^-. Because the lone pair electrons of Br^- partially distribute to H of the –C–H bond, the positive charge on H atom is reduced, resulting in a decreased force constant.[39] With increasing RH, more water disassociates the cation–anion pair, mobile Br^- appeared. The reduced interaction between [-$N(CH_3)_3^+$] and Br^- along RH caused the higher frequency shift and intensity decrease of –C–H stretching vibration band.[34] Because of the fewer [-$N(CH_3)_3^+$] groups, no –C–H stretching vibration band was apparent in PFT6-Pip-Br thin film (Figure 3d). The RH-controlled in-situ FTIR results suggest that

interactions between the cation, anion, and water differ at various RH, wherein the difference was attributed to the water adsorption and dissociation of cation–anion pairs.

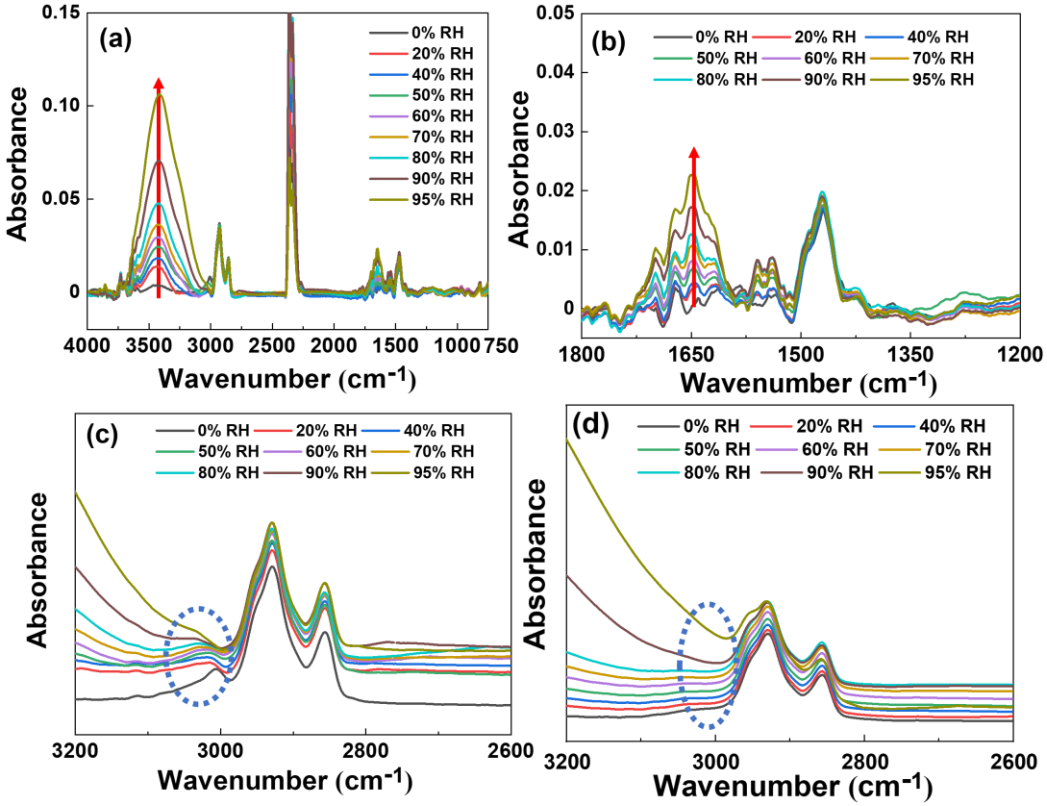

Figure 3. In situ FTIR spectra of (a, b and c) PFT6-TMA-Br and (d) PFT6-Pip-Br thin films as a function of RH: (a) wavenumber range of 750–4000 cm^{-1} of PFT6-TMA-Br thin film, (b) wavenumber range of 1200–1800 cm^{-1} of PFT6-TMA-Br thin film, (c) wavenumber range of 2600–3200 cm^{-1} of PFT6-TMA-Br thin film, and (d) wavenumber range of 2600–3200 cm^{-1} of PFT6-Pip-Br thin film. To clearly see the –C–H stretching vibration band shift, the spectra were moved along the Y-axis in Figure 3c and 3d.

3.4 Morphology of thin films.

To analyze the molecular structure of PFT6-TMA-Br and PFT6-Pip-Br thin films, RH-controlled GI-SAXS has been used. Figure 4 shows the 1D GI-SAXS profiles of PFT6-TMA-Br

and PFT6-Pip-Br thin films in dry and 95% RH conditions. No distinct scattering peak exists for PFT6-TMA-Br thin film, suggesting the amorphous structure of PFT6-TMA-Br thin film. A very weak scattering peak at q_z = 3.84 nm^{-1} (d = 1.6 nm) in the out-of-plane direction was obtained for PFT6-Pip-Br thin film at dry and 95% RH conditions. Very few organized structures were found in the PFT6-Pip-Br thin film. However, most of the region inside the PFT6-Pip-Br thin film is still amorphous.

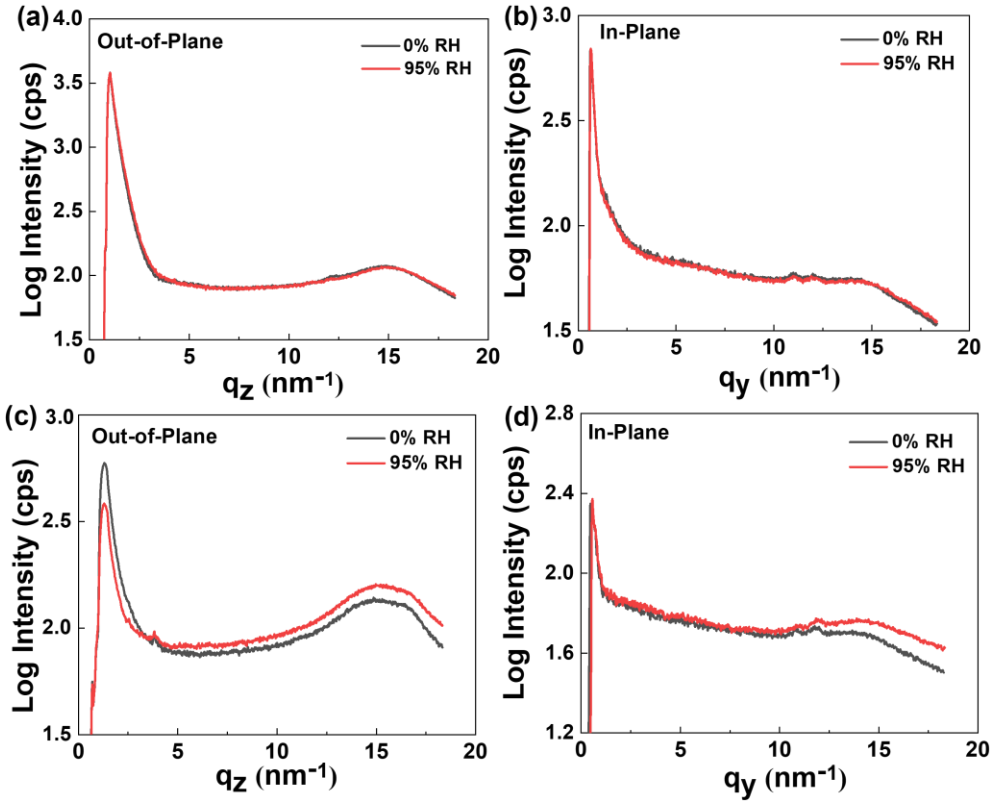

Figure 4. 1D GI-SAXS profiles in the out-of-plane and in-plane directions at 0% and 95% RH of (a and b) PFT6-TMA-Br and (c and d) PFT6-Pip-Br thin films. Scattering peaks at q_y=10.8 and 12.0 nm^{-1} originated from the Lumirror window of the humidity-controlled cell.

To confirm that the entire film has an amorphous structure, p-polarized multiple angle incidence resolution spectrometry (pMAIRS) was performed. Figure S9 exhibits the pMAIRS spectra of PFT6-TMA-Br and PFT6-Pip-Br thin films. As shown in Figure S9, the band at 1498 cm^{-1} is

assigned to the stretching vibration of the aromatic rings. For both PFT6-TMA-Br and PFT6-Pip-Br thin films, the absorbance of the aromatic ring stretching vibration in the in-plane direction is the same as that in the out-of-plane direction, suggesting an amorphous structure inside the anion exchange thin films. This amorphous structure is apparent with other reported anion exchange thin films.[3–5] GI-SAXS results suggested an amorphous structure that was reported in various hydrocarbon-based anion exchange thin films.[5] No nanophase separation or organized structure was readily apparent inside the FAA3 and QA-PPO anion exchange thin films.[3,4] Compared to proton exchange thin films, anion exchange thin films show a much weaker nanophase separation tendency. The possible reasons for the weak nanophase separation in anion exchange thin films are the lower hydrophilicity of quaternary ammonium groups than sulfonic acid groups.[40,41] It might also be caused by insufficient electron density contrast in GI-SAXS. Results reveal that the weakly organized structure inside the PFT6-Pip-Br thin film was observed. However, this might be insufficient to benefit the anion conduction.

3.5 Anion Conductivity

Elucidating OH^- conductive properties is important for AEMFCs performance because few reports have described studies of OH^- conductivity in thin film form due to the requirement of a CO_2-free atmosphere. The anion conductivity of PFT6-TMA and PFT6-Pip thin films at 25 °C is shown as a function of RH in Figure 5. Both OH^- conductivity and Br^- conductivity increased with RH, irrespective of the cationic group. As discussed in RH-controlled in situ FTIR results, with more water entering the thin film, the degree of interaction between cations and counter-anions decreased, whereas the number of mobile OH^-/Br^- increased. The increased mobile ion number and water uptake contributed to the enhanced anion conductivity along with RH. Conductivities decrease in the order of PFT6-TMA-OH (1.8×10^{-2} S cm^{-1}) > PFT6-Pip-OH (6.8×10^{-3} S cm^{-1}) >

PFT6-TMA-Br (4.3×10^{-3} S cm^{-1}) > PFT6-Pip-Br (1.5×10^{-3} S cm^{-1}). Higher OH^- conductivity than Br^- conductivity was observed within the whole RH region, which is consistent with results of our earlier work.[7] The energy dispersive X-ray spectroscopy (EDX) spectra obtained before and after ion exchange were used to confirm ion exchange processes (Fig. S10 and S11).

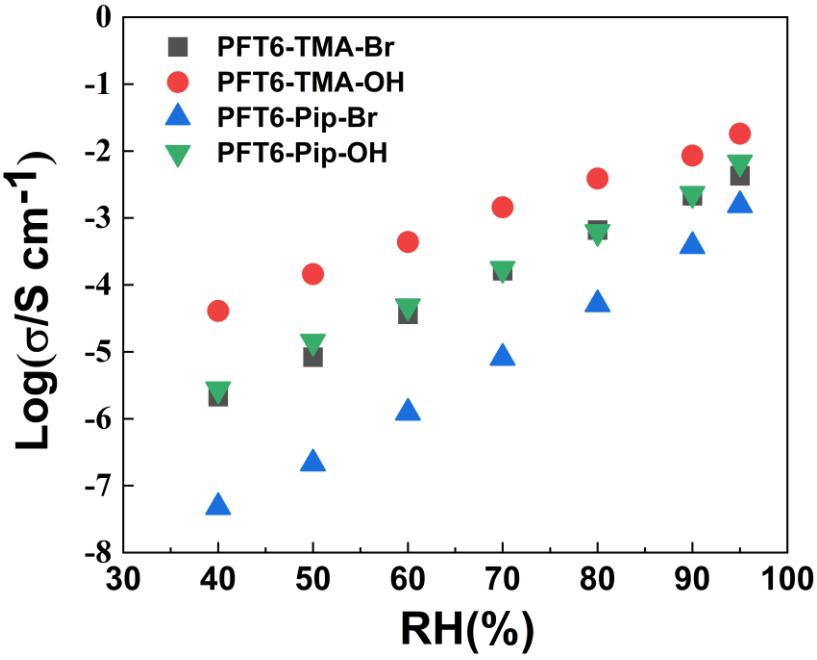

Figure 5. Anion conductivity of PFT6-TMA and PFT6-Pip thin films as a function of RH at 25 °C.

thin films were higher than HCO_3^- conductivity throughout the whole range of RH. This finding confirmed the OH^- conductivities of the PFT6-TMA-OH and PFT6-Pip-OH thin films.

The OH^- reacts easily with CO_2 in the air, which can drastically decrease conductivity. To avoid carbonation, OH^- conductivity measurement was conducted after the preparation of thin films under the protection of N_2. Furthermore, the HCO_3^- conductivity as a function of RH was investigated as shown in Figure S12. The OH^- conductivities of PFT6-TMA-OH and PFT6-Pip-OH thin films were higher than HCO_3^- conductivity throughout the whole range of RH. The ionic mobility of OH^- and HCO_3^- at infinite dilution in water are 20.64×10^{-8} m^2 s^{-1} V^{-1} and 4.61×10^{-8} m^2

s^{-1} V^{-1}, respectively.[42] The lower mobility of HCO_3^- is contribute to its lower conductivity. Besides, OH^- transport through Grotthuss mechanism under high hydration conditions. While HCO_3^- transport only through diffusion and convection even under high hydration conditions, which further lower down the HCO_3^- conductivity.[43] This finding confirmed the OH^- conductivities of the PFT6-TMA-OH and PFT6-Pip-OH thin films.

To provide further insights into the anion conduction properties of PFT6-TMA and PFT6-Pip thin films, the number of water molecule dependence of anion conductivity is presented in Figure 6. The much lower water content of Br^- form thin film than OH^- form limits comparison under the high number of water molecules. Both OH^- conductivity and Br^- conductivity increased along with the number of water molecules. Unlike the case in which the horizontal axis was RH dependent, in the low hydration range, the Br^- conductivity was even higher than OH^- conductivity for both PFT6-TMA and PFT6-Pip thin films. Similar trends only as a membrane form were obtained in other studies reported in the literature.[3,25,44] Marino and co-authors pointed out that OH^- conductivity is lower than either F^-, Cl^-, or Br^- conductivity under a low hydration range in the membrane form.[25] Peng and co-authors demonstrated that the mobility of OH^- in a Tokuyama A201 membrane is lower than Cl^- under low water content because of the hindrance of hydrogen bonding interaction with water.[44] The degree of dissociation of ion pairs significantly decreased at low hydration conditions because OH^- requires a higher hydration number than Br^- does.[25] Conductivity can be expressed by the effective mobility and concentration of mobile anion carriers as

$$\sigma = n\mu e \qquad (6)$$

where n signifies the concentration of mobile anion carriers, μ stands for the effective mobility of anion carriers, and e represents the elementary charge.[45] In this case, both the low mobile OH^-

concentration and low mobility contributed to the reduced OH^- conductivity under low hydration conditions. A high dissociation level and increase of mobile OH^- concentration can be expected for the OH^- form under high hydration conditions.[46] The high ion mobility and high OH^- concentration are attributed to the superior hydroxide conductivity at high hydration. In the few thin film literature of anion conduction, Shrivastava and co-authors found higher Br^- conductivity than F^- conductivity under a low number of water molecules in FAA3 thin films.[3] However, there was a lack of OH^- conductivity comparison of thin films. The successful measurement of OH^- conductivity in this work provides further insight into the OH^- conduction properties of thin film under low hydration conditions. The OH^- and Br^- forms of PFT6-TMA thin films exhibited much higher conductivity than each identical form of PFT6-Pip thin films at similar λ. Further discussion of various molecular properties will be undertaken after the discussion of anion transport activation energy.

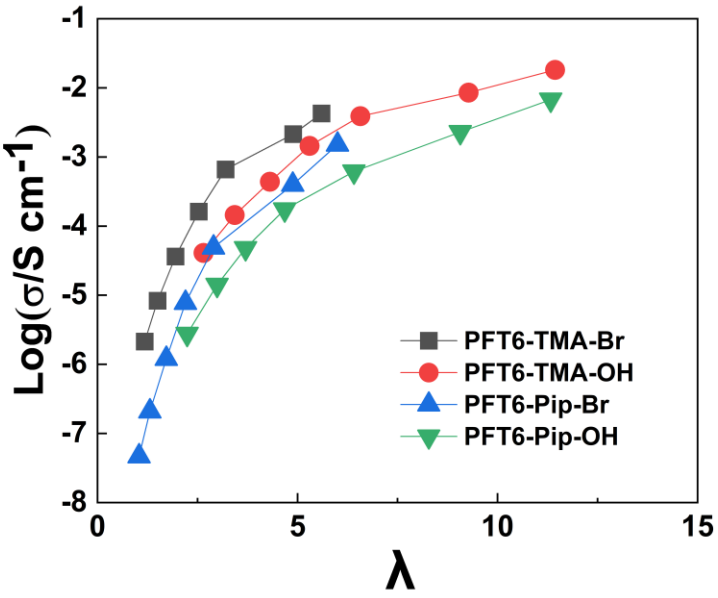

Figure 6. Anion conductivity of PFT6-TMA and PFT6-Pip thin films as a function of number of water molecules at 25°C. Lines were used as a guide to the eyes.

To investigate anion transport activation energy, in-situ temperature dependence of OH^- conductivity measurement process was developed in the thin film form using equipment constructed in-house. This report is the first to describe the OH^- transport activation energy in the anion exchange thin film form. Each Br^- and OH^- conductivity at various temperatures and 90% RH was investigated. The Br^- and OH^- conductivity of the PFT6-TMA and PFT6-Pip thin films as a function of temperatures are depicted in Figure 7. Arrhenius-type temperature dependence of the anion conductivity was observed for both PFT6-TMA and PFT6-Pip thin films at temperatures of 20–50 °C. The activation energies (E_a) were calculated as 44.6 kJ mol^{-1} for PFT6-TMA-Br thin film, 33.2 kJ mol^{-1} for PFT6-TMA-OH thin film, 49.8 kJ mol^{-1} for PFT6-Pip-Br thin film, and 35.7 kJ mol^{-1} for PFT6-Pip-OH thin film. The activation energies of OH^- conduction in both PFT6-TMA and PFT6-Pip thin films were lower than that of Br^- conduction, indicating that the energy barrier to be overcome for Br^- transport is higher than that of OH^- transport. A possible reason is that OH^- can be transported through a Grotthuss or vehicle mechanism, whereas halide can only be transported by a vehicle mechanism.[38,47–49]

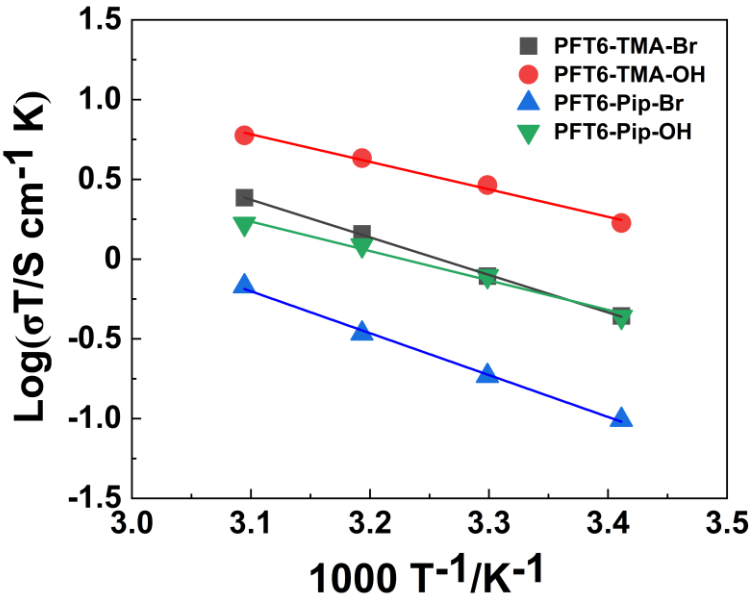

Figure 7. Arrhenius plots of anion conductivity for the PFT6-TMA and PFT6-Pip thin films under 90% RH.

The higher anion conductivity in TMA-based anion conductive polymers than that of Pip-based anion conductive polymer is apparent with other reported anion conductive polymers.[50–52] In this work, the anion conduction activation energy of PFT6-TMA thin films was comparable to PFT6-Pip thin films. As presented in Figure 6, the OH^- and Br^- forms of PFT6-TMA thin films exhibited much higher conductivity than each form of PFT6-Pip thin films at similar λ. The anion conductivity of anion exchange thin films depends on IEC, water uptake, dissociation degree of ion-pairs, morphology, conduction mechanism, hydrophobicity and the size of the cationic group. The IEC values of PFT6-TMA-OH and PFT6-Pip-OH were, respectively, 2.27 and 2.01 meq g^{-1}. As shown in the water uptake part, each identical form of PFT6-TMA and PFT6-Pip thin films exhibited a similar dissociation degree and water uptake results. Furthermore, both PFT6-TMA-Br and PFT6-Pip-Br thin films exhibited an amorphous structure. The comparable activation energy of anion conduction between PFT6-TMA and PFT6-Pip thin films suggests a similar ion conduction mechanism inside the PFT6-TMA and PFT6-Pip thin films. The hydrophobicity and size of the cationic group are respectively more hydrophobic and bulkier in Pip. According to the analysis above, we can propose that a higher IEC, lower hydrophobicity, and the smaller size of TMA are attributable to the higher anion conductivity of PFT6-TMA thin films than of each identical form of PFT6-Pip thin films at similar λ.

This work investigated the OH^- conduction properties of fluorene-thiophene-based anion conductive polymers in thin film form with different cationic groups, especially the OH^- conduction activation energy was revealed for the first time as thin film form. Similar OH^- conduction activation energy was observed in PFT6-TMA-OH and PFT6-Pip-OH thin films,

suggesting the same OH^- conduction mechanism in fluorene-thiophene-based thin films with different cationic groups though the OH^- conductivity was different. Higher IEC, lower hydrophobicity, and smaller size of TMA contribute superior OH^- conductivity of the PFT6-TMA-OH thin film.

CONCLUSIONS

After high-performance fluorene-thiophene-based anion exchange thin films were prepared for this study, the hydration properties, anion conduction properties, and morphology of poly(fluorene-thiophene)-based thin films with different cationic groups were investigated. OH^- form thin films of PFT6-TMA and PFT6-Pip exhibited higher water uptake than their corresponding Br^- form thin films at the same RH. Water uptake results imply that the anions, rather than cations, dominate the hydration properties of anion exchange thin film. Anion conduction properties of anion exchange thin films depend on the number of water molecules. Higher OH^- conductivity than Br^- conductivity is apparent under high hydration conditions with enhanced ion mobility and full dissociation, although Br^- conductivity was higher than OH^- conductivity under the low number of water molecules. Higher IEC, along with less hydrophobicity and smaller size of TMA, contributed to the higher conductivity of PFT6-TMA thin films. Under 90% RH, PFT6-TMA and PFT6-Pip thin films exhibited similar activation energies for anion conduction in each anionic form. This result provides the first detailed information about anion exchange thin films in OH^- form, which is expected to benefit the development of efficient anion exchange thin film.

ASSOCIATED CONTENT

Supporting Information

Detailed experiment-related information and results about nuclear magnetic resonance (^{1}H NMR), gel permeation chromatography (GPC), attenuated total reflection FTIR (ATR-FTIR) spectroscopy, thermogravimetric analyzer (TGA), ion exchange capacity (IEC), scanning Electron Microscope and Energy Dispersive X-ray Spectroscopy (SEM-EDX), and p-Polarized multiple angle incidence resolution spectrometry (pMAIRS) is presented in Supporting Information.

AUTHOR INFORMATION

Corresponding Author

Yuki Nagao - School of Materials Science Japan Advanced Institute of Science and Technology 1-1 Asahidai, Nomi, Ishikawa 923-1292, Japan; Email: ynagao@jaist.ac.jp Phone: +81(Japan)-761-51-1541

Authors

Fangfang Wang - School of Materials Science Japan Advanced Institute of Science and Technology 1-1 Asahidai, Nomi, Ishikawa 923-1292, Japan

Shusaku Nagano - College of Science, Rikkyo University, Tokyo 171-8501, Japan

Mitsuo Hara - Department of Molecular & Macromolecular Chemistry, Nagoya University, Nagoya 464-8603, Japan

Notes

The authors declare no competing financial interest.

ACKNOWLEDGMENT

This work was supported by Mitani Foundation for Research and Development, The Murata Science Foundation, JSPS KAKENHI Grant Number JP18K05257, 21H00020, and 21H01997, and JST CREST Grant Number JPMJCR21B3, Japan.

REFERENCES

(1) Alaswad, A.; Palumbo, A.; Dassisti, M.; Olabi, A. G. *Fuel Cell Technologies, Applications, and State of the Art. A Reference Guide*; Elsevier Ltd., 2016. https://doi.org/10.1016/b978-0-12-803581-8.04009-1.

(2) Varcoe, J. R.; Atanassov, P.; Dekel, D. R.; Herring, A. M.; Hickner, M. A.; Kohl, P. A.; Kucernak, A. R.; Mustain, W. E.; Nijmeijer, K.; Scott, K.; Xu, T.; Zhuang, L. Anion-Exchange Membranes in Electrochemical Energy Systems. *Energy Environ. Sci.* **2014**, *7* (10), 3135–3191. https://doi.org/10.1039/c4ee01303d.

(3) Shrivastava, U. N.; Zhegur-Khais, A.; Bass, M.; Willdorf-Cohen, S.; Freger, V.; Dekel, D. R.; Karan, K. Water Content and Ionic Conductivity of Thin Films of Different Anionic Forms of Anion Conducting Ionomers. *J. Phys. Chem. C* **2020**, *124* (43), 23469–23478. https://doi.org/10.1021/acs.jpcc.0c04278.

(4) Kushner, D. I.; Zhu, L.; Kusoglu, A.; Hickner, M. A. Side Chain Influence on the Mechanical Properties and Water Uptake of Confined Comb-Shaped Cationic Polymer Thin Films. *Macromol. Chem. Phys.* **2016**, *217* (21), 2442–2451. https://doi.org/10.1002/macp.201600254.

(5) Luo, X.; Kushner, D. I.; Li, J.; Park, E. J.; Kim, Y. S.; Kusoglu, A. Anion Exchange Ionomers : Impact of Chemistry on Thin-Film Properties. *Adv. Funct. Mater.* **2021**, *2008778*, 1–12. https://doi.org/10.1002/adfm.202008778.

(6) Kimura, T.; Kawamoto, T.; Aoki, M.; Mizusawa, T.; Yamada, N. L.; Miyatake, K.; Inukai, J. Sublayered Thin Films of Hydrated Anion Exchange Ionomer for Fuel Cells Formed on SiO_2 and Pt Substrates Analyzed by Neutron Reflectometry under Controlled Temperature and Humidity Conditions. *Langmuir* **2020**, *36* (18), 4955–4963. https://doi.org/10.1021/acs.langmuir.0c00440.

(7) Wang, F.; Wang, D.; Nagao, Y. OH^- Conductive Properties and Water Uptake of Anion Exchange Thin Films. *ChemSusChem* **2021**, *14*, 2694–2697. https://doi.org/10.1002/cssc.202100711.

(8) Zhang, F.; Li, T.; Chen, W.; Wu, X.; Yan, X.; Xiao, W.; Zhang, Y.; Wang, X.; He, G. Electron-Donating C-NH_2 Link Backbone for Highly Alkaline and Mechanical Stable Anion Exchange Membranes. *ACS Appl. Mater. Interfaces* **2021**, *13* (8), 10490–10499. https://doi.org/10.1021/acsami.1c00324.

(9) Li, L.; Wang, J. A.; Ma, L.; Bai, L.; Zhang, A.; Qaisrani, N. A.; Yan, X.; Zhang, F.; He, G. Dual-Side-Chain-Grafted Poly(Phenylene Oxide) Anion Exchange Membranes for Fuel-Cell and Electrodialysis Applications. *ACS Sustain. Chem. Eng.* **2021**. https://doi.org/10.1021/acssuschemeng.1c02189.

(10) Chen, N.; Hu, C.; Wang, H. H.; Kim, S. P.; Kim, H. M.; Lee, W. H.; Bae, J. Y.; Park, J. H.; Lee, Y. M. Poly(Alkyl-Terphenyl Piperidinium) Ionomers and Membranes with an Outstanding Alkaline-Membrane Fuel-Cell Performance of 2.58 W Cm^{-2}. *Angew. Chemie - Int. Ed.* **2021**, *60* (14), 7710–7718. https://doi.org/10.1002/anie.202013395.

(11) Liu, X.; Wu, D.; Liu, X.; Luo, X.; Liu, Y.; Zhao, Q.; Li, J.; Dong, D. Perfluorinated Comb-Shaped Cationic Polymer Containing Long-Range Ordered Main Chain for Anion Exchange Membrane. *Electrochim. Acta* **2020**, *336*, 135757. https://doi.org/10.1016/j.electacta.2020.135757.

(12) Li, N.; Guiver, M. D.; Binder, W. H. Towards High Conductivity in Anion-Exchange Membranes for Alkaline Fuel Cells. *ChemSusChem* **2013**, *6* (8), 1376–1383. https://doi.org/10.1002/cssc.201300320.

(13) Couture, G.; Alaaeddine, A.; Boschet, F.; Ameduri, B. Polymeric Materials as Anion-Exchange Membranes for Alkaline Fuel Cells. *Prog. Polym. Sci.* **2011**, *36* (11), 1521–1557. https://doi.org/10.1016/j.progpolymsci.2011.04.004.

(14) Noh, S.; Jeon, J. Y.; Adhikari, S.; Kim, Y. S.; Bae, C. Molecular Engineering of Hydroxide Conducting Polymers for Anion Exchange Membranes in Electrochemical Energy Conversion Technology. *Acc. Chem. Res.* **2019**, *52* (9), 2745–2755. https://doi.org/10.1021/acs.accounts.9b00355.

(15) Lee, W. H.; Park, E. J.; Han, J.; Shin, D. W.; Kim, Y. S.; Bae, C. Poly(Terphenylene) Anion Exchange Membranes: The Effect of Backbone Structure on Morphology and Membrane Property. *ACS Macro Lett.* **2017**, *6* (5), 566–570. https://doi.org/10.1021/acsmacrolett.7b00148.

(16) Merle, G.; Wessling, M.; Nijmeijer, K. Anion Exchange Membranes for Alkaline Fuel Cells: A Review. *J. Memb. Sci.* **2011**, *377* (1–2), 1–35. https://doi.org/10.1016/j.memsci.2011.04.043.

(17) Pan, D.; Olsson, J. S.; Jannasch, P. Poly(Fluorene Alkylene) Anion Exchange Membranes with Pendant Spirocyclic and Bis-Spirocyclic Quaternary Ammonium Cations. *ACS Appl. Energy Mater.* **2021**. https://doi.org/10.1021/acsaem.1c03359.

(18) Lee, W. H.; Mohanty, A. D.; Bae, C. Fluorene-Based Hydroxide Ion Conducting Polymers for Chemically Stable Anion Exchange Membrane Fuel Cells. *ACS Macro Lett.* **2015**, *4* (4), 453–457. https://doi.org/10.1021/acsmacrolett.5b00145.

(19) Pan, D.; Olsson, J. S.; Jannasch, P. Poly(Fluorene Alkylene) Anion Exchange Membranes with Pendant Spirocyclic and Bis-Spirocyclic Quaternary Ammonium Cations. *ACS Appl. Energy Mater.* **2022**, *5* (1), 981–991. https://doi.org/10.1021/acsaem.1c03359.

(20) Soni, R.; Miyanishi, S.; Kuroki, H.; Yamaguchi, T. Pure Water Solid Alkaline Water Electrolyzer Using Fully Aromatic and High-Molecular-Weight Poly(Fluorene-Alt-Tetrafluorophenylene)-Trimethyl Ammonium Anion Exchange Membranes and Ionomers. *ACS Appl. Energy Mater.* **2021**, *4*, 1053–1058. https://doi.org/10.1021/acsaem.0c01938.

(21) Salma, U.; Nagao, Y. Alkaline Stability of Ether Bond Free Fluorene-Based Anion Exchange Polymer Containing Cycloaliphatic Quaternary Ammonium Groups. *Polym. Degrad. Stab.* **2020**, *179*, 109299. https://doi.org/10.1016/j.polymdegradstab.2020.109299.

(22) Lin, C. X.; Huang, X. L.; Guo, D.; Zhang, Q. G.; Zhu, A. M.; Ye, M. L.; Liu, Q. L. Side-Chain-Type Anion Exchange Membranes Bearing Pendant Quaternary Ammonium Groups: Via Flexible Spacers for Fuel Cells. *J. Mater. Chem. A* **2016**, *4* (36), 13938–13948. https://doi.org/10.1039/c6ta05090e.

(23) Dang, H. S.; Jannasch, P. Exploring Different Cationic Alkyl Side Chain Designs for Enhanced Alkaline Stability and Hydroxide Ion Conductivity of Anion-Exchange

Membranes. *Macromolecules* **2015**, *48* (16), 5742–5751. https://doi.org/10.1021/acs.macromol.5b01302.

(24) Luo, X.; Rojas-Carbonell, S.; Yan, Y.; Kusoglu, A. Structure-Transport Relationships of Poly(Aryl Piperidinium) Anion-Exchange Membranes: Eeffect of Anions and Hydration. *J. Memb. Sci.* **2020**, *598*, 117680. https://doi.org/10.1016/j.memsci.2019.117680.

(25) Marino, M. G.; Melchior, J. P.; Wohlfarth, A.; Kreuer, K. D. Hydroxide, Halide and Water Transport in a Model Anion Exchange Membrane. *J. Memb. Sci.* **2014**, *464*, 61–71. https://doi.org/10.1016/j.memsci.2014.04.003.

(26) Sun, Z.; Lin, B.; Yan, F. Anion-Exchange Membranes for Alkaline Fuel-Cell Applications: The Effects of Cations. *ChemSusChem* **2018**, *11* (1), 58–70. https://doi.org/10.1002/cssc.201701600.

(27) Lin, B.; Qiu, L.; Qiu, B.; Peng, Y.; Yan, F. A Soluble and Conductive Polyfluorene Ionomer with Pendant Imidazolium Groups for Alkaline Fuel Cell Applications. *Macromolecules* **2011**, *44* (24), 9642–9649. https://doi.org/10.1021/ma202159d.

(28) Kusoglu, A.; Weber, A. Z. New Insights into Perfluorinated Sulfonic-Acid Ionomers. *Chem. Rev.* **2017**, *117* (3), 987–1104. https://doi.org/10.1021/acs.chemrev.6b00159.

(29) Marcus, Y. A Simple Empirical Model Describing the Thermodynamics of Hydration of Ions of Widely Varying Charges, Sizes, and Shapes. *Biophys. Chem.* **1994**, *51* (2–3), 111–127. https://doi.org/10.1016/0301-4622(94)00051-4.

(30) Israelachvili, J. N. Interactions Involving Polar Molecules. *Intermol. Surf. Forces* **2011**, 71–90. https://doi.org/10.1016/b978-0-12-375182-9.10004-1.

(31) Ralph G. Pearson. Hard and Soft Acids and Bases. *J. Am. Chem. Soc.* **1963**, *265* (C), 3533–3539.

(32) Kreuer, K. D. The Role of Internal Pressure for the Hydration and Transport Properties of Ionomers and Polyelectrolytes. *Solid State Ionics* **2013**, *252*, 93–101. https://doi.org/10.1016/j.ssi.2013.04.018.

(33) Nagao, Y.; Tanaka, T.; Ono, Y.; Suetsugu, K.; Hara, M.; Wang, G.; Nagano, S.; Abe, T. Introducing Planar Hydrophobic Groups into an Alkyl-Sulfonated Rigid Polyimide and How This Affects Morphology and Proton Conductivity. *Electrochim. Acta* **2019**, *300*, 333–340. https://doi.org/10.1016/j.electacta.2019.01.118.

(34) Vico, S.; Palys, B.; Buess-Herman, C. Hydration of a Polysulfone Anion-Exchange Membrane Studied by Vibrational Spectroscopy. *Langmuir* **2003**, *19* (8), 3282–3287. https://doi.org/10.1021/la026290+.

(35) Xu, Z.; Li, H.; Wang, C.; Pan, H.; Han, S. The Methyl C-H Blueshift in N, N-Dimethylformamide-Water Mixtures Probed by Two-Dimensional Fourier-Transform Infrared Spectroscopy. *J. Chem. Phys.* **2006**, *124* (24). https://doi.org/10.1063/1.2206177.

(36) Kar, B.; Bardhan, S.; Ghosh, P.; Ganguly, B.; Kundu, K.; Sarkar, S.; Paul, B. K.; Das, S. A Fast and Additive Free C–C Homo/Cross-Coupling Reaction in Reverse Micelle: An Understanding of Role of Surfactant, Water Content and Base on the Product Yield and Reaction Site. *ChemistrySelect* **2017**, *2* (3), 1079–1088. https://doi.org/10.1002/slct.201601986.

(37) Vandiver, M. A.; Caire, B. R.; Pandey, T. P.; Li, Y.; Seifert, S.; Kusoglu, A.; Knauss, D. M.; Herring, A. M.; Liberatore, M. W. Effect of Hydration on the Mechanical Properties and Ion Conduction in a Polyethylene-b-Poly(Vinylbenzyl Trimethylammonium) Anion Exchange Membrane. *J. Memb. Sci.* **2016**, *497*, 67–76. https://doi.org/10.1016/j.memsci.2015.09.034.

(38) Pandey, T. P.; Maes, A. M.; Sarode, H. N.; Peters, B. D.; Lavina, S.; Vezzù, K.; Yang, Y.; Poynton, S. D.; Varcoe, J. R.; Seifert, S.; Liberatore, M. W.; Di Noto, V.; Herring, A. M. Interplay between Water Uptake, Ion Interactions, and Conductivity in an e-Beam Grafted Poly(Ethylene-Co-Tetrafluoroethylene) Anion Exchange Membrane. *Phys. Chem. Chem. Phys.* **2015**, *17* (6), 4367–4378. https://doi.org/10.1039/c4cp05755d.

(39) Gussoni, M.; Castiglioni, C. Infrared Intensities. Use of the CH-Stretching Band Intensity as a Tool for Evaluating the Acidity of Hydrogen Atoms in Hydrocarbons. *J. Mol. Struct.* **2000**, *521* (1–3), 1–18. https://doi.org/10.1016/S0022-2860(99)00421-4.

(40) Knauth, P.; Pasquini, L.; Narducci, R.; Sgreccia, E.; Becerra-Arciniegas, R. A.; Di Vona, M. L. Effective Ion Mobility in Anion Exchange Ionomers: Relations with Hydration, Porosity, Tortuosity, and Percolation. *J. Memb. Sci.* **2021**, *617*, 118622. https://doi.org/10.1016/j.memsci.2020.118622.

(41) Bharath, V. J.; Millichamp, J.; Neville, T. P.; Mason, T. J.; Shearing, P. R.; Brown, R. J. C.; Manos, G.; Brett, D. J. L. Measurement of Water Uptake in Thin-Film Nafion and Anion Alkaline Exchange Membranes Using the Quartz Crystal Microbalance. *J. Memb. Sci.* **2016**, *497*, 229–238. https://doi.org/10.1016/j.memsci.2015.09.027.

(42) Yohtaro, T. K. Y. Effects of CO_2 Concentration and Electric Current on the Ionic Conductivity of Anion Exchange Membranes for Fuel Cells. *Electrochemistry* **2011**, *2*, 94–97. https://doi.org/10.1016/s1071-3581(04)00339-3.

(43) Ziv, N.; Mustain, W. E.; Dekel, D. R. The Effect of Ambient Carbon Dioxide on Anion-Exchange Membrane Fuel Cells. *ChemSusChem* **2018**, *11* (7), 1136–1150. https://doi.org/10.1002/cssc.201702330.

(44) Peng, J.; Roy, A. L.; Greenbaum, S. G.; Zawodzinski, T. A. Effect of CO2 Absorption on Ion and Water Mobility in an Anion Exchange Membrane. *J. Power Sources* **2018**, *380*, 64–75. https://doi.org/10.1016/j.jpowsour.2018.01.071.

(45) Arof, A. K.; Amirudin, S.; Yusof, S. Z.; Noor, I. M. A Method Based on Impedance Spectroscopy to Determine Transport Properties of Polymer Electrolytes. *Phys. Chem. Chem. Phys.* **2014**, *16* (5), 1856–1867. https://doi.org/10.1039/C3CP53830C.

(46) Haynes, W. M. *CRC Handbook of Chemistry and Physics, 93rd Edition*; 100 Key Points; Taylor \& Francis, 2012.

(47) Chen, C.; Tse, Y. L. S.; Lindberg, G. E.; Knight, C.; Voth, G. A. Hydroxide Solvation and Transport in Anion Exchange Membranes. *J. Am. Chem. Soc.* **2016**, *138* (3), 991–1000. https://doi.org/10.1021/jacs.5b11951.

(48) Sarode, H. N.; Vandiver, M. A.; Liu, Y.; Maes, A.; Pandey, T. P.; Ertem, S. P.; Tsai, T.; Zhang, B.; Herbst, D.; Linberg, G.; Tse, Y.-L. S.; Seifert, S.; Di Noto, V.; Coughlin, E. B.; Yan, Y.; Voth, G.; Witten, T.; Knauss, D. M.; Liberatore, M. W.; Herring, A. M. Thin Robust Anion Exchange Membranes for Fuel Cell Applications. *ECS Meet. Abstr.* **2014**, *MA2014-02* (21), 1259–1259. https://doi.org/10.1149/ma2014-02/21/1259.

(49) Miyanishi, S.; Yamaguchi, T. Highly Conductive Mechanically Robust High Mw Polyfluorene Anion Exchange Membrane for Alkaline Fuel Cell and Water Electrolysis Application. *Polym. Chem.* **2020**, *11* (23), 3812–3820. https://doi.org/10.1039/D0PY00334D.

(50) Koronka, D.; Otsuji, K.; Matsumoto, A.; Miyatake, K.; Miyatake, K. Partially Fluorinated Copolymers Containing Pendant Piperidinium Head Groups as Anion Exchange

Membranes for Alkaline Fuel Cells. *RSC Adv.* **2019**, *9* (64), 37391–37402. https://doi.org/10.1039/c9ra07775h.

(51) Allushi, A.; Pham, T. H.; Olsson, J. S.; Jannasch, P. Ether-Free Polyfluorenes Tethered with Quinuclidinium Cations as Hydroxide Exchange Membranes. *J. Mater. Chem. A* **2019**, *7* (47), 27164–27174. https://doi.org/10.1039/c9ta09213g.

(52) Yang, K.; Li, X.; Guo, J.; Zheng, J.; Li, S.; Zhang, S.; Cao, X.; Sherazi, T. A.; Liu, X. Preparation and Properties of Anion Exchange Membranes with Exceptional Alkaline Stable Polymer Backbone and Cation Groups. *J. Memb. Sci.* **2020**, *596*, 117720. https://doi.org/10.1016/j.memsci.2019.117720.

For Table of Contents Only